MEMS pressure sensor with an AlGaN/GaN based high electron mobility transistor

G. Vanko*, J. Dzuba*, I. Rýger*, M. Vallo* and T. Lalinský*

*Institute of Electrical Engineering, Slovak Academy of Sciences, Bratislava, Slovakia, gabriel.vanko@savba.sk

ABSTRACT

This work deals with technology of MEMS piezoelectric pressure sensors based high electron mobility transistors (HEMTs) integrated on AlGaN/GaN membranes able to work in harsh environments. The originality of the concept proposal consists in research of new progressive thin layers based on metal oxides and/or their combinations for Schottky gate sensing electrodes and methods of bulk micromachining of the substrate material in order to get free-standing AlGaN/GaN micromechanic structures.

Keywords: piezoelectricity, HEMT, micromachining, harsh environment, pressure sensing

1 INTRODUCTION

Group III-Nitrides (III-N) are very attractive for pressure and strain sensor applications due to their excellent piezoelectric properties [1]. HEMTs but also Schottky diodes and resistors based on AlGaN/GaN heterostructures could be very useful as sensing devices, especially for application in harsh environment or at high temperatures (e.g. the wings of an aircraft, in combustion engine, exhaust etc.) [2]. To investigate piezo-response of these devices the following approaches were currently reported: (a) a bulk device approach; (b) devices integrated on a bulk substrate cantilevers; (c) devices integrated on membrane structures. The first approach (a) does not require the realization of suspended microstructures. The function is based on the action of hydrostatic pressure which alters Ni/AlGaN Schottky barrier height [3], the internal fields in GaN/AlGaN/GaN heterostructures [4] and the polarization in AlGaN/GaN heterostructure [5]. These effects are relatively small compared to the strain sensors exposed to bending. Thus, the realized sensor is sensitive to high pressure and the high mechanical stability of this structure favours such applications. The performance can be controlled by the gate voltage and highest sensitivity is achieved close to the pinch-off [5]. In the second approach (b) AlGaN/GaN HEMT process technology is performed on a bulk sapphire substrate. The substrate with the integrated HEMT as a strain sensor is then cut out into a bulk cantilever structure. This structure is then exposed to bending [6-11]. The resulting channel resistivity is measured in dependence on applied strain. It can be concluded from the obtained results that the interaction between piezoelectric and piezoresistive properties improves the sensitivity of pressure sensors by using AlGaN/GaN heterostructures with confined 2DEG. In contrast to SiC, the potential of group of III-nitrides for pressure sensors based on membrane structures integrated with HEMT sensing device (c) is much less evaluated. The difficulty to fabricate suspended AlGaN/GaN heterostructure arises from the high chemical stability of group III-nitrides, which complicates the necessary undercutting techniques. A promising approach is the deposition of AlGaN/GaN heterostructure on Si. Despite the high prospects of the 2DEG for mechanical sensors with internal amplification, only a few reports on membrane test structures are available [1, 12-14].

In this work, we describe the processing technology and demonstrate MEMS piezoelectric pressure sensor based on HEMT as a sensing device integrated on an AlGaN/GaN diaphragm. The pressure sensor presented in this article can work on two principles. First one is the piezoelectric pressure sensor which reacts to the external pressure load by generating of piezoelectric charge on its electrodes. The second, HEMT principle uses the change of 2DEG channel conductivity with the applied external loading [15-18]. The charge accumulation in the channel is particularly caused by piezoelectric and spontaneous polarization which can be changed by external mechanical load [19].

2 DESIGN AND TECHNOLOGY

A cross-section view through the MEMS pressure sensors based on C-HEMT sensing device integrated on the circular AlGaN/GaN membrane is shown in Fig. 1. To fabricate the micromachined sensor structure, the front-side processing of the HEMT device is combined with bulk silicon micromachining. This will be described in the following sections.

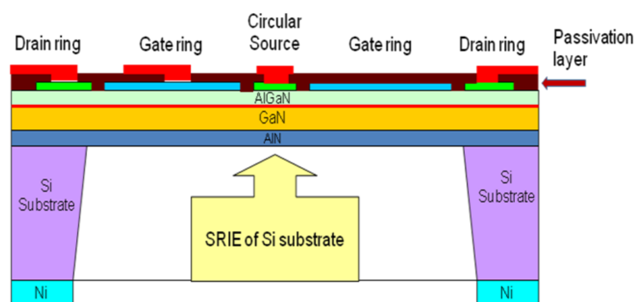

Figure 1: Cross-section view of the proposed MEMS piezoelectric pressure sensor.

2.1 Modeling and simulation

The model of the sensor has been developed in the 3D finite element method (FEM) software Ansys. Stressed state of any membrane can be achieved using several different approaches in Ansys. We can simply prescribe the displacement on the outer radius of model while its centre remains constrained.

The pre-stressed state from first step of simulation was taken as an initial state in the piezoelectric analysis. Bottom electrode was created by the conductive 2DEG channel at AlGaN/GaN interface while the top one is formed by the Schottky gate electrode deposited on the AlGaN surface. Because of high loading pressure, large deflections were expected and therefore nonlinear solution was turned on. Static pressure load applied from substrate side of the model varies from 0.1 to 50 kPa. Piezoelectric induced charge (as the response to pressure load) is captured on the ring electrode and its dependence on pressure is shown in Fig. 2. From these results, the residual stress suppression seems to be crucial to obtain piezoelectric MEMS pressure sensor with high detection sensitivity. It should be noted that total accumulated piezoelectric charge depends on the position and area of the sensing electrode. In the next step, optimization of these two input variables is performed.

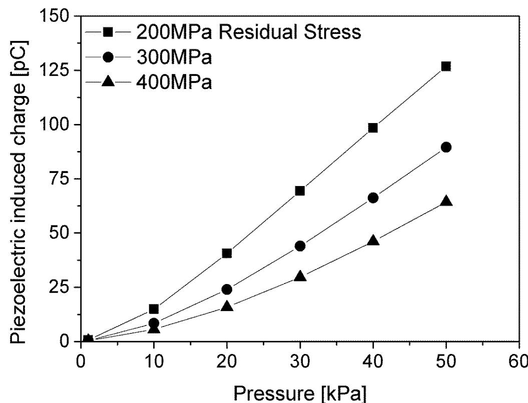

Figure 2: Simulated piezoelectric charge vs. pressure with varying residual stress (200-400 MPa).

In this simulation, the electrode with constant width (5 μm) was chosen and its central radius was continuously increased in each simulation. Pressure of 10 kPa was taken as constant load of the sensor membrane. The dependence of induced charge on position of the electrode was then obtained (Fig. 3). We found that induced charge depends on central radius of electrode (what is practically the "position of electrode"). Figure 3 shows the change in polarity of the charge if the electrode crosses the critical position near to the clamping. It is caused by change in behaviour of mechanical stress (from tensile to compressive or vice versa) on the membrane surface at this position (neutral-stress point).

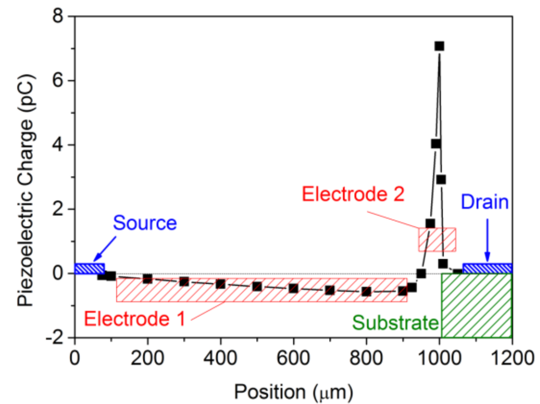

Figure 3: Induced piezoelectric charge vs. position of electrode (circular membrane, there is the Source electrode with the reserved area in the centre of membrane).

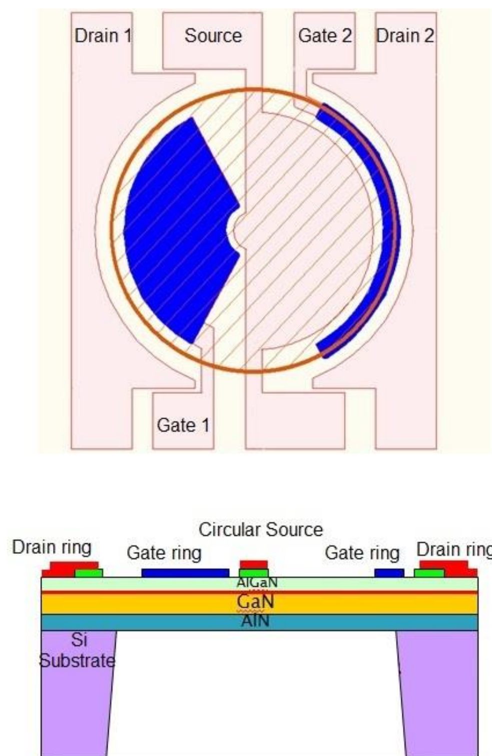

Figure 4: Modified topology of membrane pressure sensor with two different positioned sensing electrodes (top) and schematic cross-section view of sensor device (bottom, circular topology).

From the simulations it is clear that stress on top of the AlGaN layer on the membrane varies around residual stress. Variation is caused by stress changes at the top and bottom surface of a membrane with fixed edges [20]. In our simulation, if the residual stress state is considered as an initial state, the top surface of the membrane becomes strained differently depending on distance from the

membrane centre. The surface near the membrane centre is strained positively (elongation) meanwhile that near to the membrane edge is strained negatively (shortening). Inverted strain causes stress variation in radial direction and therefore generating piezoelectric charge of opposite sign. Neutral stress points (points where surface stress goes to zero – in this case to residual stress value) in our model is located approximately at the distance 930 µm from the membrane centre. Results led us to use two electrodes in location with maximal induced charge with both polarities. Optimal locations for prescribed loading (10 kPa) and boundary conditions were determined: 70-900 µm and 950-1050 µm for the first and second sensing electrode, respectively. Top view of these ring gate sensing electrodes and schematic cross-section of the related MEMS sensor structure is shown in Fig. 4.

2.2 Heterostructure growth

The large lattice mismatch and the difference in thermal expansion coefficients between GaN and Si substrate leads to the formation of cracks or stress generation [21]. We investigated the residual stress and maximal loading of the AlGaN/GaN diaphragms by two independent methods. The tensile stress was estimated to be around 21 MPa for the fabricated diaphragms. The low values of stress demonstrate the recent progress in epitaxial growth of stress free GaN layers on Si substrate.

An undoped AlGaN/GaN heterostructure, grown by metal-organic chemical vapor-phase deposition (MOCVD) on a 300 µm thick silicon substrate, is used in our processing technology. The thickness of the AlGaN barrier layer and the GaN buffer (membrane) layer is 20 nm and 4.2 µm, respectively. The aluminum mole fraction of the AlGaN is nominally set to 0.25.

2.3 Contact metallization

As reported in the literature [22], Ti/Al/Ni/Au is the most commonly used metallic system to form ohmic source and drain contacts in AlGaN/GaN based HEMTs. Few years ago, we presented a solution to lower the specific contact resistivity and improve the surface morphology that are crucial to achieve the required electrical parameters of fabricated electronic devices. We found out that adding a thin Nb layer into the conventional metallization stack and alloying at optimal annealing conditions can significantly lower both contact resistivity and transfer length while the surface roughness is practically eliminated.

The refractory metals such as Ru, Ir and their conducting metal oxides have a great potential for high temperature stable Schottky gate formation on AlGaN/GaN heterostructure which defines a HEMT device. The measured I-V characteristics of the Ir based Schottky contacts (as deposited and fabricated by thermal oxidation process at different temperatures of oxidation) are depicted in Figure 5. IrO_2 gates of AlGaN/GaN HEMTs have shown an increased Schottky barrier (Φ>1.23 eV) and lowered leakage current (I_g<$1x10^{-10}$ A) with thermally stable gate interface what is a necessary condition for reliable and stable operation of the transistors in the role of electronic and sensor elements.

Finally, Ti/Au metallic layers are patterned on the top of the alloyed ohmic contacts and Schottky ring gate contact layers to improve the device bonding and interconnection. The metallic leads are connected with the bonding pads that are placed outside the etched area

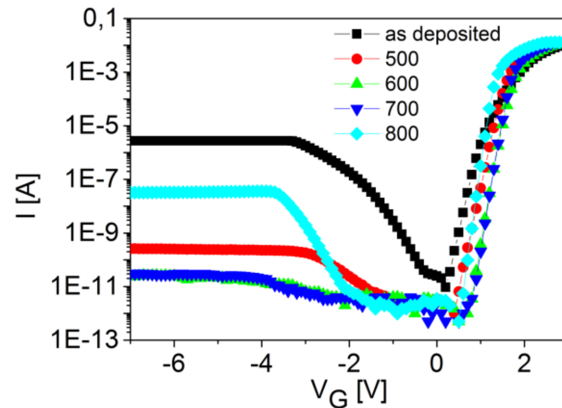

Figure 5: I-V characteristics of 15 nm thick iridium layer oxidized in O2 ambient at 500-900 °C for 1 min.

2.4 Insulation

To prevent electrical shortening between the electrodes of HEMTs and the top metallic leads, an effective insulation has to be ensured. We proposed two different ways to achieve the desired goal. First, an appropriate MESA type etching of the AlGaN layer in the selected areas can be applied. It uses the selective reactive ion etching in CCl_4 plasma for approximately 2 min. The desired depth of etch is 100-150 nm. In the second approach, a whole area deposition of an insulating Si_3N_4 layer with a subsequent etching in the defined areas again through a photoresist mask is used.

2.5 Bulk micromachining of substrate

The final technological step in the fabrication process of the AlGaN/GaN membrane-like sensor structure is the deep reactive ion etching (DRIE) of the 330 µm thick bearing Si substrate. DRIE has been performed in a time-multiplexed inductively coupled plasma (ICP) reactor with SF_6 (for etching) and C_4F_8 (for sidewall passivation) gas mixture. The AlN interfacial layer serves as the etch-stop layer of the trench-free silicon etching. Low frequency pulsing bias power is used to minimize destructive etching effects at the membrane base.

3 SENSOR DEMONSTRATION

After the AlGaN/GaN membrane were fabricated (shown in Fig. 6), the preliminary experiments were made to demonstrate the sensor functionality. First, we measured the value of the drain current at various bias conditions without any loading. After applying dynamic pressure load (with frequency f=20Hz) on the membrane the corresponding amplitude of the charge change was measured. It is depicted in Fig. 7. The obtained results are gained from the inner big sensing electrode and a good correlation with simulations was achieved. Next step will be the comprehensive characterization of the sensing devices with various electrode dimensions and in wide frequency range. After the optimization of the growth process we can expect further improvment in sensitivity of the device due to the suppressed residual stress in the membrane.

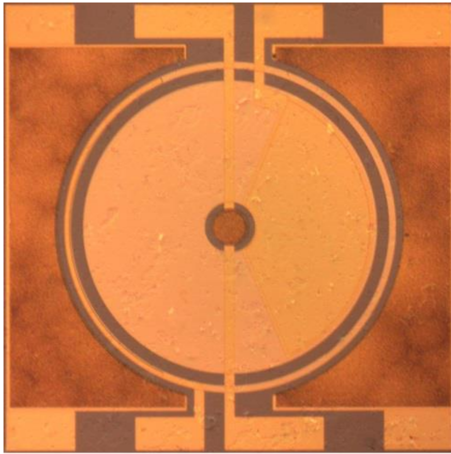

Figure 6: Real view of the fabricated MEMS piezoelectric pressure sensor with metallizations on the top and through a Si_3N_4 insulation layer

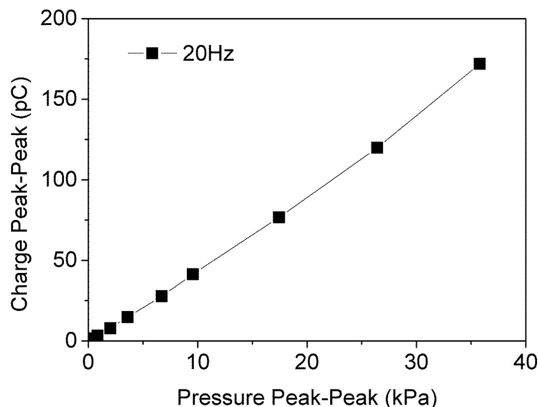

Figure 7: Induced piezoelectric charge vs. pressure measured at 20Hz of loading frequency.

ACKNOWLEDGEMENT

This work was supported by the Slovak Research and Development Agency under the contract No. APVV-0455-12 and APVV-0450-10.

REFERENCES

[1] V. Cimalla, J. Petzoldt and O. Ambacher, J. Phys. D: Appl. Phys. vol. 40, pp. 6386-6434 (2007)

[2] S. J. Pearton, B.S. Kang, S. Kim, F. Rena, B. P. Gila, C. R. Abernathy, J. Phys.: Condens. Matter vol. 16, pp. 961–994 (2004)

[3] Y. Liu, M.Z. Kauser, P.P. Ruden, Z. Hassan, Y. C. Lee, S. S. Ng and F. K. Yam, Appl. Phys. Lett. 88 , 022109 (2006)

[4] Y. Liu, et al., J. Appl. Phys. 99 , 113706 (2006)

[5] Y. Liu, P.P. Ruden, J. Xie, H. Morkoc and K. A. Son, Appl. Phys. Lett. 88, 013505 (2006)

[6] M. Eickhoff, O. Ambacher, G. Krötz and M. Stutzmann, J. Appl. Phys. 90, 3383 (2001)

[7] B. S. Kang, et.al., Appl. Phys. Lett. 83, 4845 (2003)

[8] Ch.- T. Chang, Sh.-K. Hsiao, E. Y. Chang, Ch.-Y. Lu, J.-Ch. Huang and Ch.-T. Lee, IEEE Electron Device Lett. 30, 213 (2009)

[9] G. Vanko, et al., Sensors & Actuators A: Physical 172 (2011) 98-102.

[10] T. Lalinský, et al., Microelectr. Engn. 88 (2011) 2424-2426.

[11] T. Lalinský, et al., Sensors and Actuators A: Physical 172 (2011) 386-391.

[12] T. Zimmermann, et al., IEEE Electron Device Lett. 27, 309 (2006)

[13] T. Lalinský, et al., Microelectron. Engn. 98 (2012) 578–581.

[14] G. Vanko, et al., Microelectron. Engn. 110 (2013) 260-264.

[15] S.N.G. Chu, et al., Mat. Sci. Eng. A-Struct. 409 (2005), pp. 340-347.

[16] R.P. Strittmatter, R.A. Beach, J. Brooke, E.J. Preisler, G.S. Picus, T.C. McGill, J. Appl Phys. 93, 5675 (2003).

[17] B.S. Kang, et al., Appl. Phys. Lett. 85, 2962 (2004).

[18] F. Bernardini, V. Fiorentini, D. Vanderbilt, Phys. Rev. B 56 (1997), R10024-10027.

[19] H. Morkoç, R. Cingolani, B. Gil, Solid-State Electron. 43 (1999), pp. 1909-1927.

[20] J.K. Olsen, "Piezoelectric Components in Microfluidic Devices," MSc Thesis, Technical university of Denmark, Denmark 2007.

[21] L. Liu, J.H. Edgar, Material Science and Engineering R 37 (2002) 61-127, A review journal, p. 93-95.

[22] N. Chaturvedi, U. Zeimer, J. Würfl and G. Tränkle, Semicond. Sci. Technol. 21,175, 2006.